Modeling and simulation of diffusion MRI signal in biological tissue

Institut national de recherche en informatique et en automatique (INRIA)

Centre Saclay (Equipe-projet DEFI)
Centre Nancy (Equipe-projet TOSCA)

Coordinateur: Jing-Rebecca Li

Participants: Houssem Haddar, Armin Leichleiter, Antoine Lejay

PhD: Dang Van Nguyen

Commissariat à l'Énergie Atomique (CEA)

Neurospin

Coordinateur: Cyril Poupon

Participants: Denis LeBihan

PhD: Benoit Schmitt, Alice Lebois, Hang Tuan Nguyen

- Modeling by PDEs
  Simulation of PDEs
- Probabilist processes
  Simulation by Monte-Carlo
- Inverse problems

- Simulation by Monte-Carlo
- MRI data acquisition
- Bio-physics

Magnetic resonance imaging

1,5Tesla magnet
(15000 Gauss)

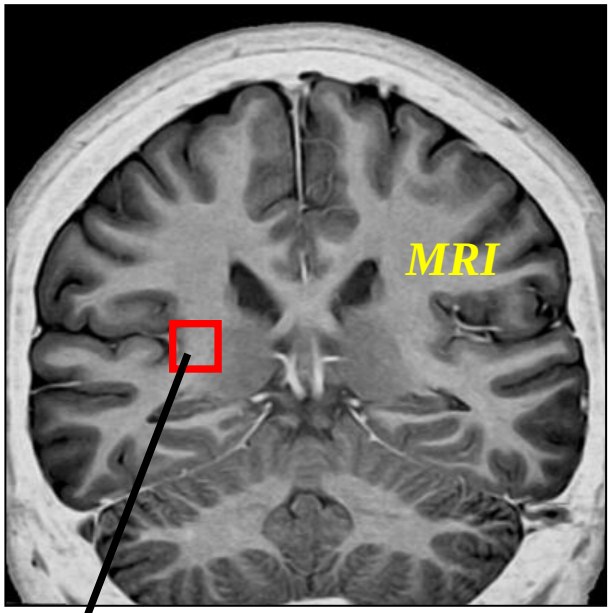

One voxel = O(mm)

Contrast: (tissue structure)

1. water magnetization (spin density)

2. relaxation (T1,T2,T2*)

3. water displacement (diffusion)

in each voxel

Diffusion MRI

Human visual cortex

(Le Bihan et al. PNAS 2006).

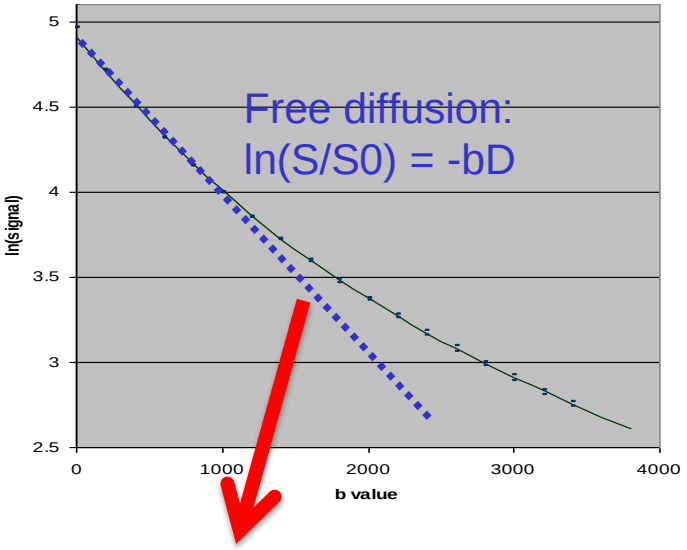

Slope is ADC (apparent diffusion coefficient)

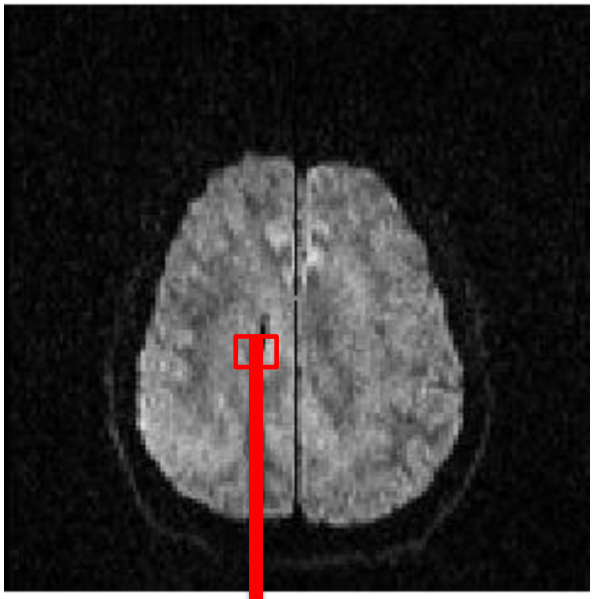

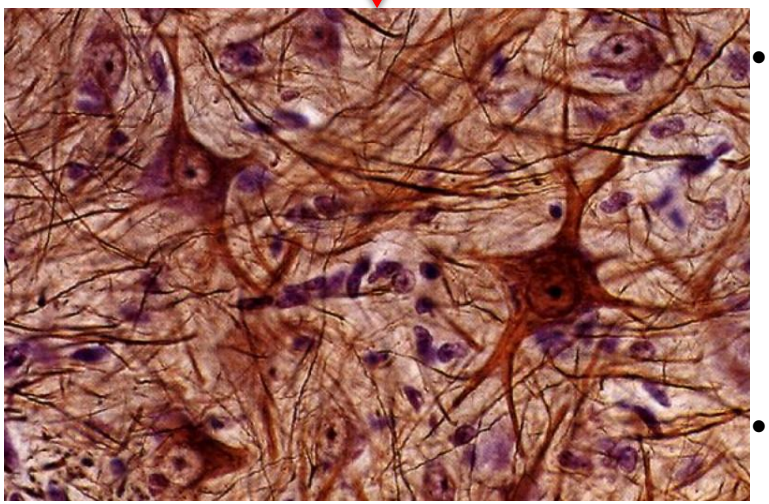

- **Diffusion MRI can measure displacement of water**
- **Displacement of water can tell us about cellular structure**
- **Understanding of biomechanics of cells, structure of brain**
- **Potential clinical value**
  - **Structure change in diseases**
  - **cells swell immediately after stroke.**
- **Functional studies**

Apply magnetic fields

Stejskal-Tanner (diffusion gradient) sequence
Also called PGSE sequence

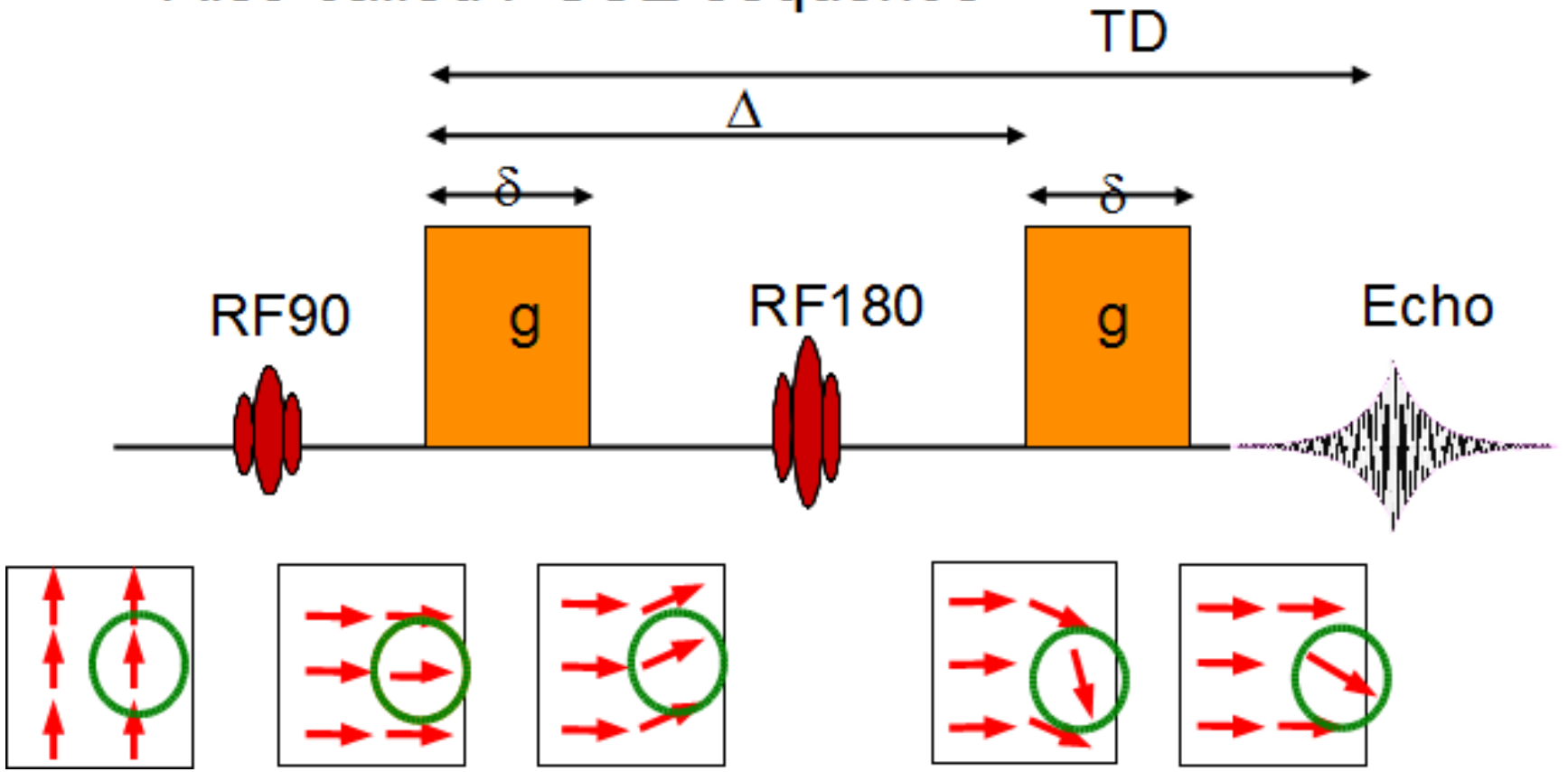

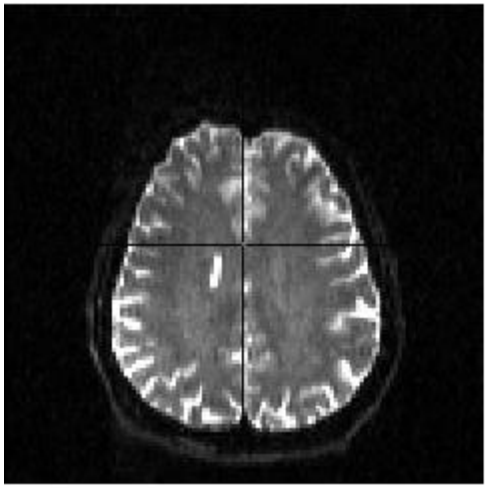

T2

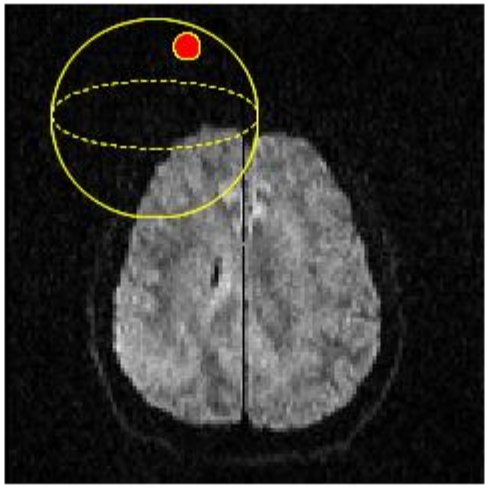

Diffusion
Orientation 1

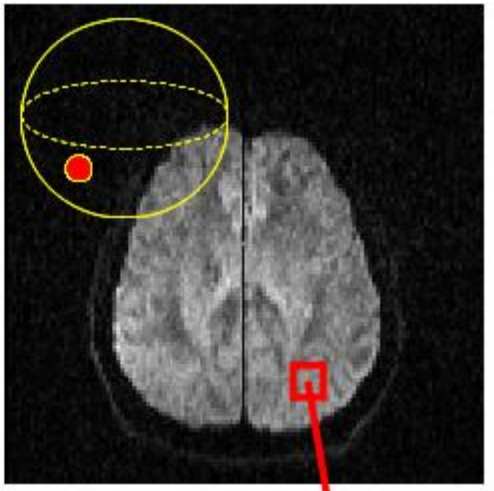

Diffusion
Orientation 2

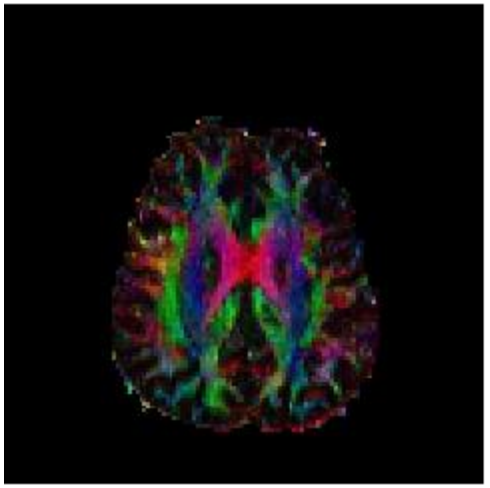

Computed fiber orientations

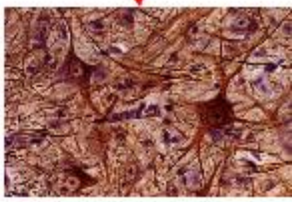

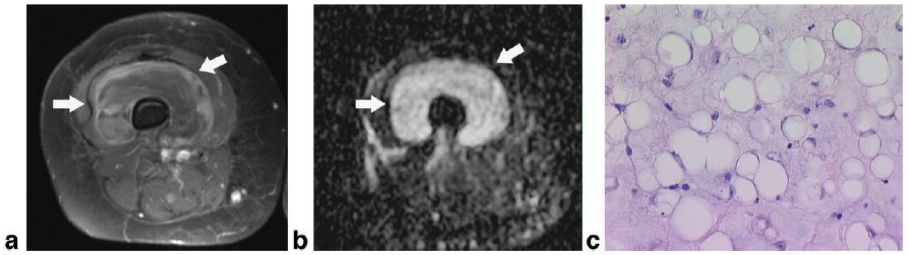

Figure 1. A 55-year-old patient with a G1 myxoid liposarcoma at the right thigh. **a:** Gadolinium-enhanced T1W MRI shows a well-defined pseudoencapsulated mass with inhomogeneously enhancing areas at the tumor margins. **b:** Corresponding ADC map of DWI displays almost unrestricted intratumoral diffusion indicating low cellularity (minimum ADC value = 201 × 10^{-3} ± 13 × 10^{-3} mm^2/second). **c:** Photomicrograph of the specimen confirms low tumor cellularity with a large proportion of vacuoles. The average cell count was 23 cells per 0.01 mm^2 (hematoxylin-eosin stain; original magnification ×400).

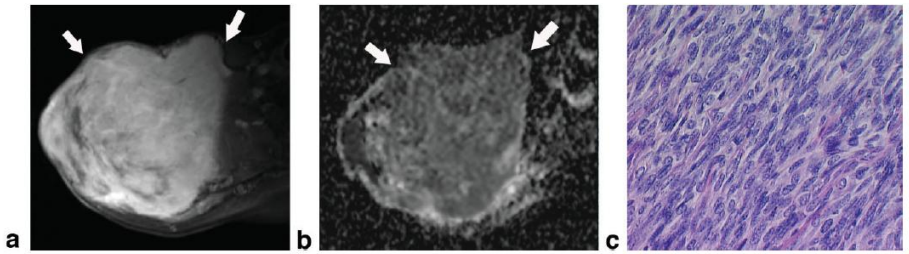

Figure 2. A 74-year-old patient with a G3 synovial sarcoma of the right shoulder. **a:** Gadolinium-enhanced T1W MRI shows a large well-enhancing mass with clear tumor margins. **b:** Corresponding ADC map of DWI displays markedly restricted intratumoral diffusion indicating high cellularity (minimum ADC value = 41 × 10^{-3} ± 21 × 10^{-3} mm^2/second). **c:** Photomicrograph of the specimen confirms a dense cellular tumor with an average cell count of 107 cells per 0.01 mm^2 (hematoxylin-eosin stain; original magnification ×400).

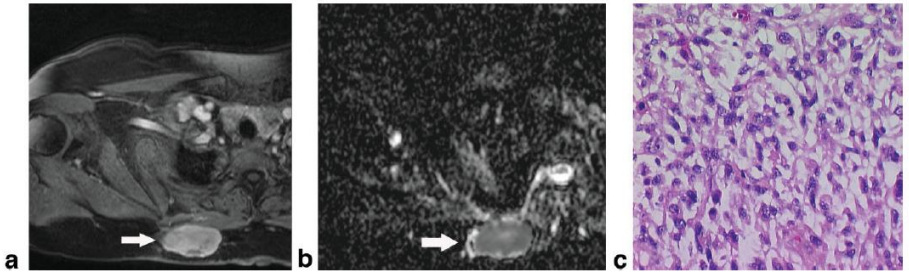

Figure 3. A 65-year-old patient with a G2 myxofibrosarcoma of the upper posterior chest wall. **a:** Gadolinium-enhanced T1W image shows an almost homogeneously-enhancing subcutaneous mass. **b:** Corresponding ADC map of DWI displays moderately restricted intratumoral diffusion indicating intermediate cellularity (minimum ADC value 96 × 10^{-3} ± 12 × 10^{-3} mm^2/second). **c:** Photomicrograph of the specimen confirms moderate tumor cellularity with an average cell count of 64 cells per 0.01 mm^2 (hematoxylin-eosin stain; original magnification ×400).

JOURNAL OF MAGNETIC RESONANCE IMAGING 29:1355–1359 (2009)

Original Research

Diffusion-Weighted Echo-Planar Magnetic Resonance Imaging for the Assessment of Tumor Cellularity in Patients With Soft-Tissue Sarcomas

Dirk Schnapauff, MD,[1*] Martin Zeile, MD,[2] Manuel Ben Niederhagen, MD,[3] Barbara Fleige, MD,[3] Per-Ulf Tunn, MD,[4] Bernd Hamm, MD,[1] and Oliver Dudeck, MD[1,2]

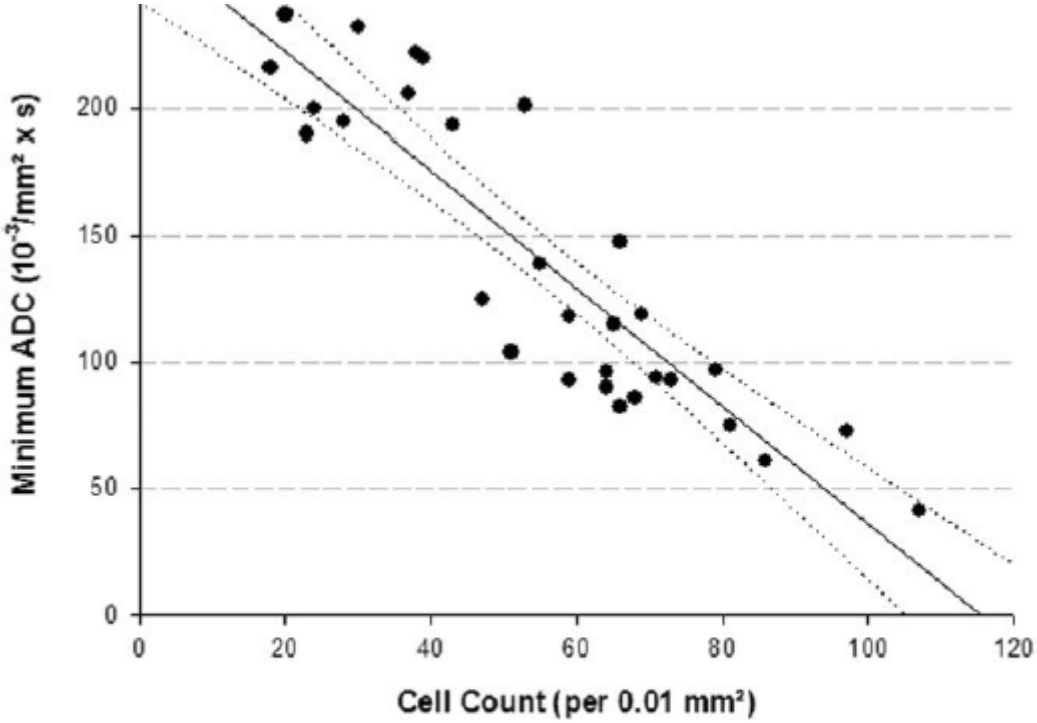

Figure 4. Relationship between minimum ADC and tumor cellularity. In musculoskeletal soft-tissue sarcomas, minimum ADC correlates well with tumor cellularity (r = −0.88; 95% CI = −0,76 to −0.96; r^2 = 0.77). Straight line indicates regression line, dotted lines denote 95% CI.

JOURNAL OF MAGNETIC RESONANCE IMAGING 31:538–548 (2010)

Original Research

Validation of Functional Diffusion Maps (fDMs) as a Biomarker for Human Glioma Cellularity

Benjamin M. Ellingson, PhD,[1,2] Mark G. Malkin, MD, FRCPC,[1,3,4] Scott D. Rand, MD, PhD,[1,2] Jennifer M. Connelly, MD,[3] Carolyn Quinsey, BS,[4] Pete S. LaViolette, MS,[5] Devyani P. Bedekar, MS,[2] and Kathleen M. Schmainda, PhD[1,2,5*]

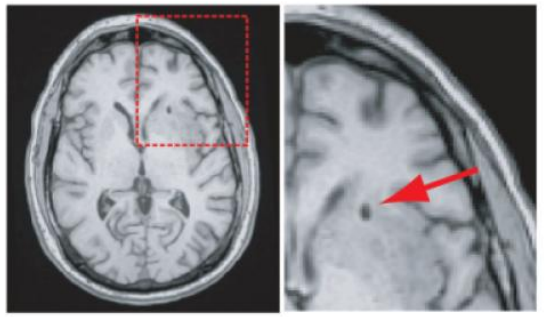

A

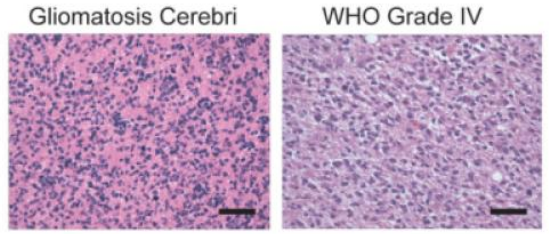

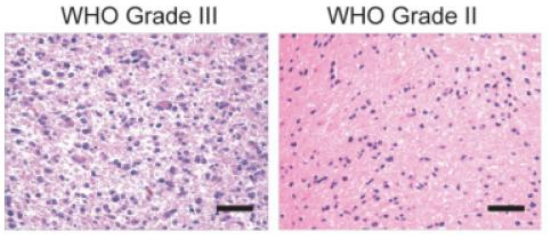

B

C

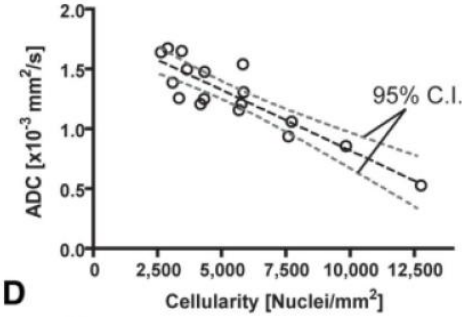

D

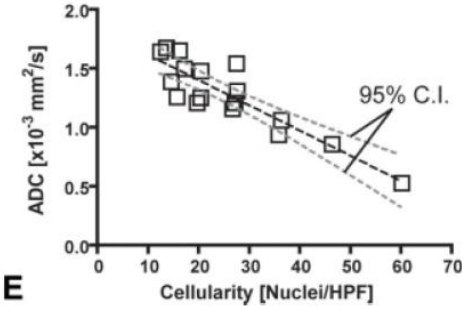

E

Figure 2. Correlation between spatially matched ADC measurements and cell density from stereotactic biopsy samples. **A:** Postoperative, high-resolution 3D T1-weighted anatomical MR images showing the biopsy location in a single patient. **B:** Representative histological images (hematoxylin & eosin, ×20 magnification) showing how cell density increases with an increase in tumor grade (scale bar = 50 μm). **C:** Spatially matched ADC measurements taken from the biopsy location in the same four patients as in B, showing a decrease in ADC with an increase in tumor grade and cell density. **D:** Scatter plot of average ADC within stereotactic biopsy locations and average cellularity for 17 patients (circles) shows a significant linear correlation (Pearson's correlation coefficient, $r^2 = 0.7933$; $P < 0.0001$) between mean ADC and mean cell density in nuclei/mm^2. **E:** Correlation between mean ADC and mean cell density in nuclei per HPF. Dashed black line = linear regression line; dashed gray lines = 95% confidence intervals for the regression.

996 • The Journal of Neuroscience, January 20, 2010 • 30(3):996–1002

Neurobiology of Disease

In Vivo Diffusion Tensor Imaging and Histopathology of the Fimbria-Fornix in Temporal Lobe Epilepsy

Luis Concha,[1] Daniel J. Livy,[2] Christian Beaulieu,[1]* B. Matt Wheatley,[3] and Donald W. Gross[4]*
[1]Department of Biomedical Engineering, [2]Faculty of Medicine and Dentistry, Division of Anatomy, [3]Department of Surgery, Division of Neurosurgery, and [4]Department of Medicine, Division of Neurology, University of Alberta, Edmonton, Alberta, Canada T6G 2B7

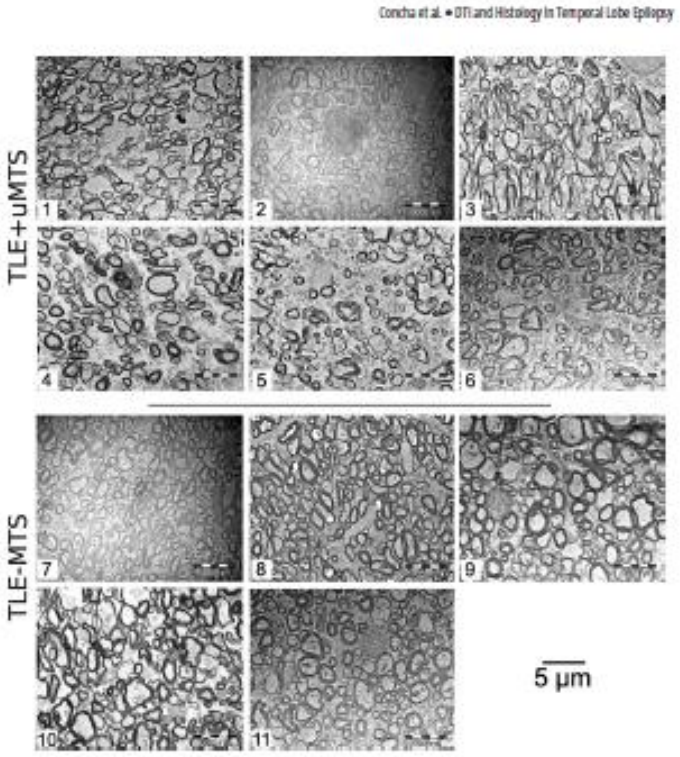

Figure 2. Electron micrographs of the fimbria-fornix. For each of the six TLE + uMTS and five TLE − MTS patients, one of the 10 available electron microscopy fields is displayed at a magnification of 3500×. Patients with mesial temporal sclerosis show fewer axons and increased extra-axonal space. Patients are identified by numbers (Table 1). Patients 5 and 8 are shown in Figure 3.

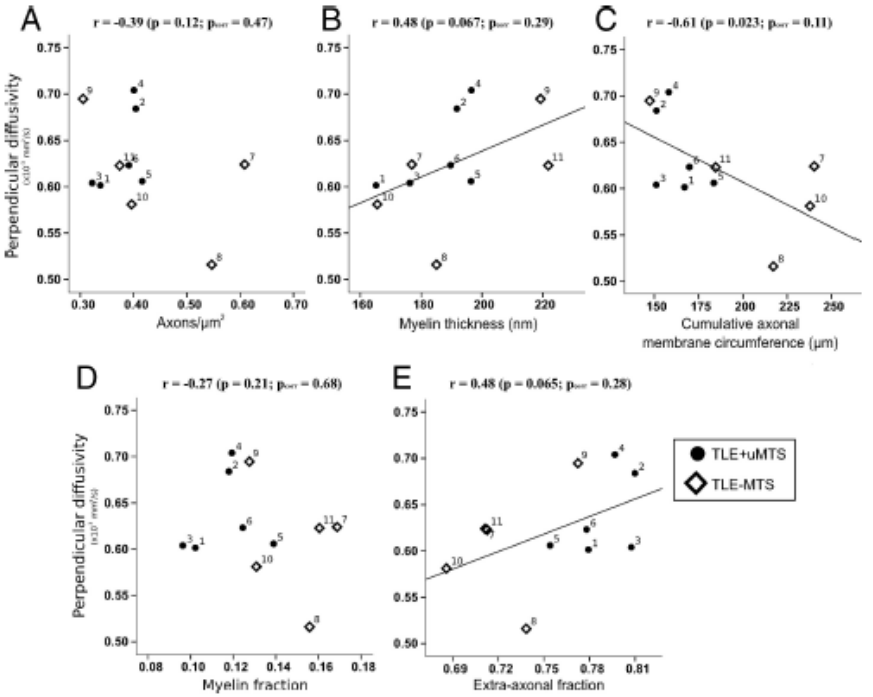

Figure 5. Histological correlates of perpendicular diffusivity in the fimbria-fornix versus axon density (***A***), myelin thickness (***B***), cumulative membrane circumference (***C***), myelin fraction (***D***), and extra-axonal fraction (***E***). Cumulative axonal membrane circumference (***C***) from electron microscopy of the smaller specimen of the fimbria-fornix adjacent to the hippocampus shows a trend toward a negative correlation with perpendicular diffusivity from the entire ipsilateral crus of the fimbria-fornix. The perpendicular diffusion appears to be driving the anisotropy changes reported in Figure 4*C*. Numbers identify each patient (Table 1).

Step 1. Simulation

Human visual cortex

(Le Bihan et al. PNAS 2006).

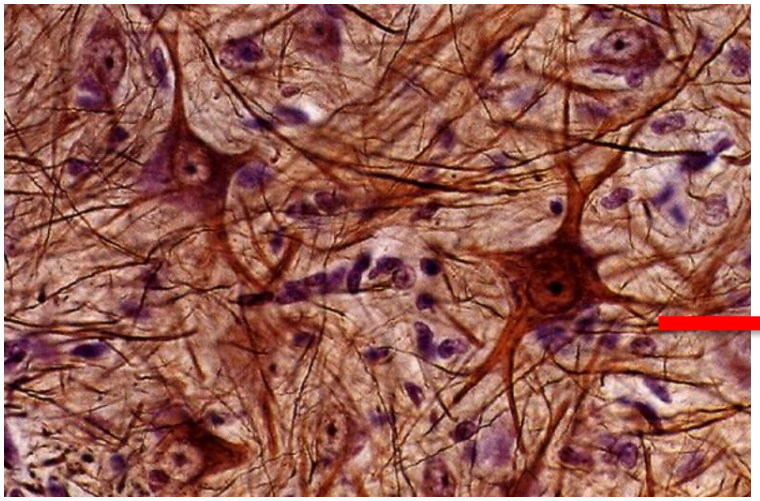

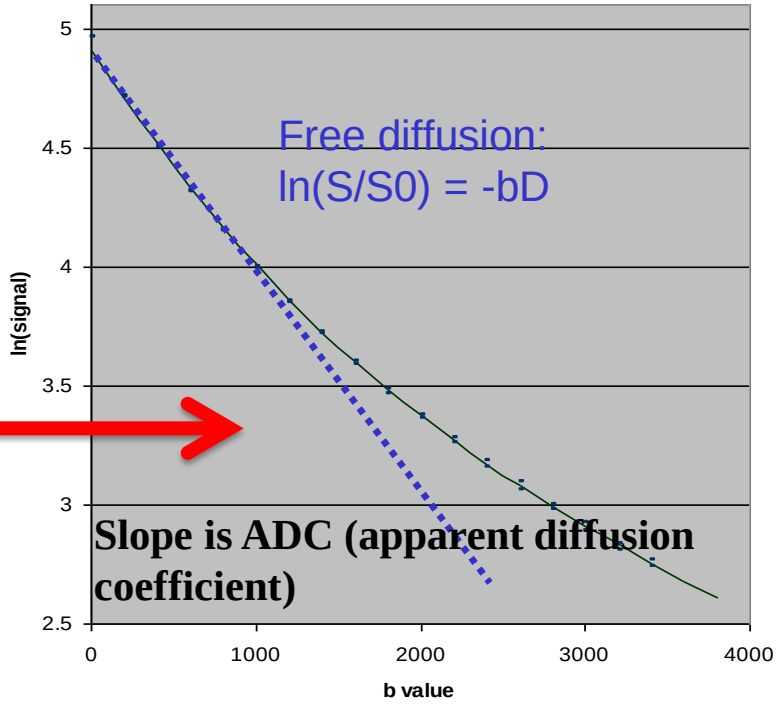

Later: inverse problem

Step 1. Simulation

- Partial differential equation model “Bloch-Torrey PDE”
- Permeable membranes
- Simpler cellular geometry
- Easier theoretical analysis

- Monte-Carlo simulation of random walkers, representing concentrated mass of water molecules.
- Impermeable membranes for now.
- More flexible cellular geometry

Bloch-Torrey PDE
2or 3 compartment diffusion model

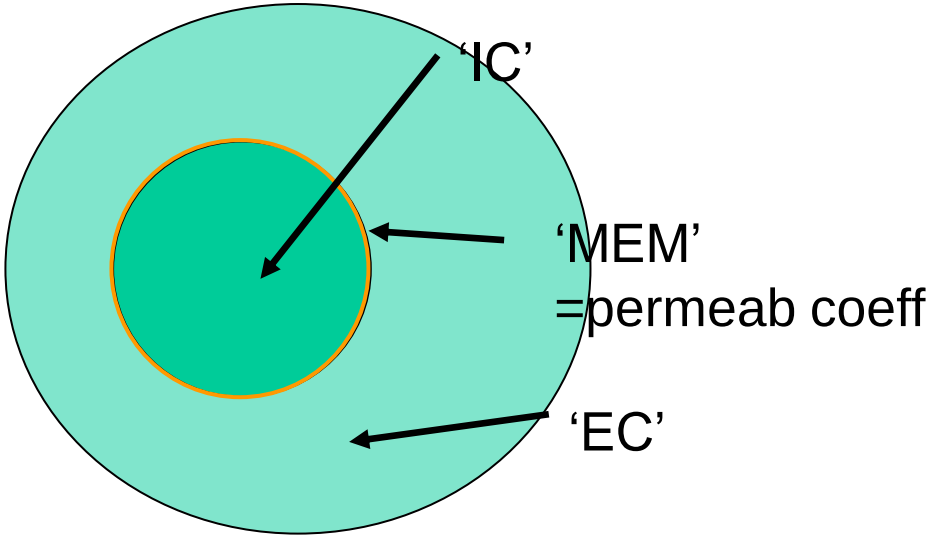

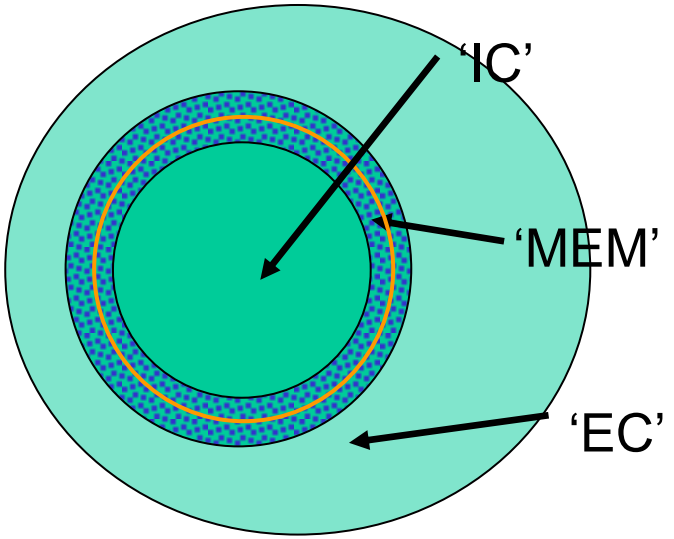

IC, EC: Intra-, extracellular space
MEM: membrane-bound layer

$$\frac{\partial M(\vec{x},t,\vec{x}_0)}{\partial t} = -i\, f(t)\, \gamma\, \vec{g}\cdot\vec{x}\, M(\vec{x},t|\vec{x}_0) + \nabla\cdot(D\nabla M(\vec{x},t|\vec{x}_0)),$$

$$M(\vec{x},0|\vec{x}_0) = \delta(\vec{x}-\vec{x}_0)$$

FVforDMRI: written in Fortran90,
C++ version in development
10000 lines.
Authors: Jing-Rebecca Li, Dang Van Nguyen

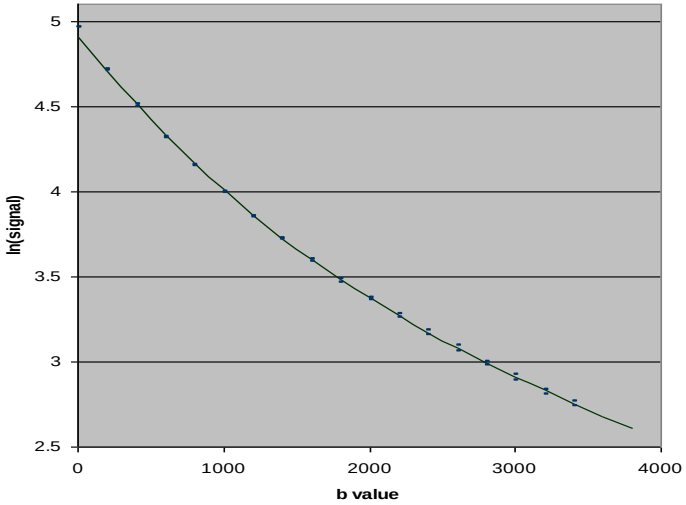

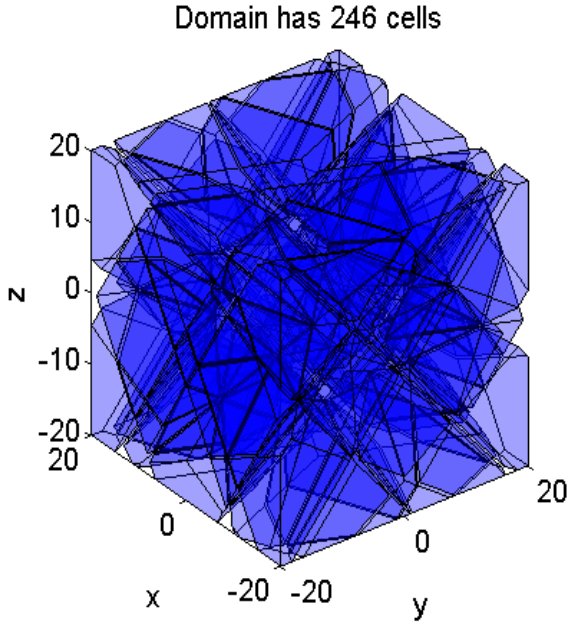

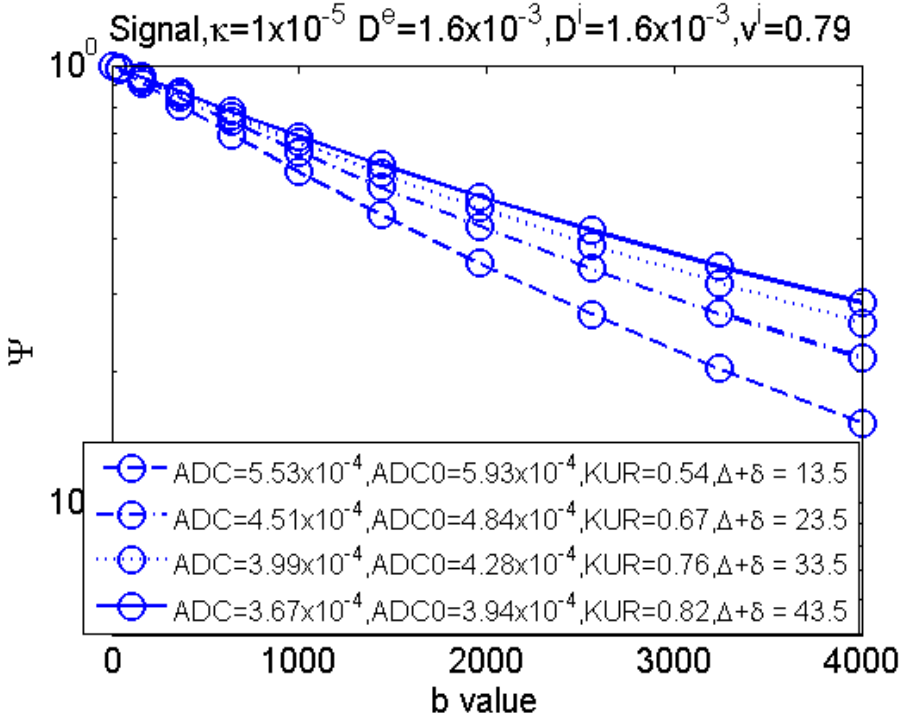

Simulation by FVforDMRI of
Diffusion MRI signals
in complicated cellular environment

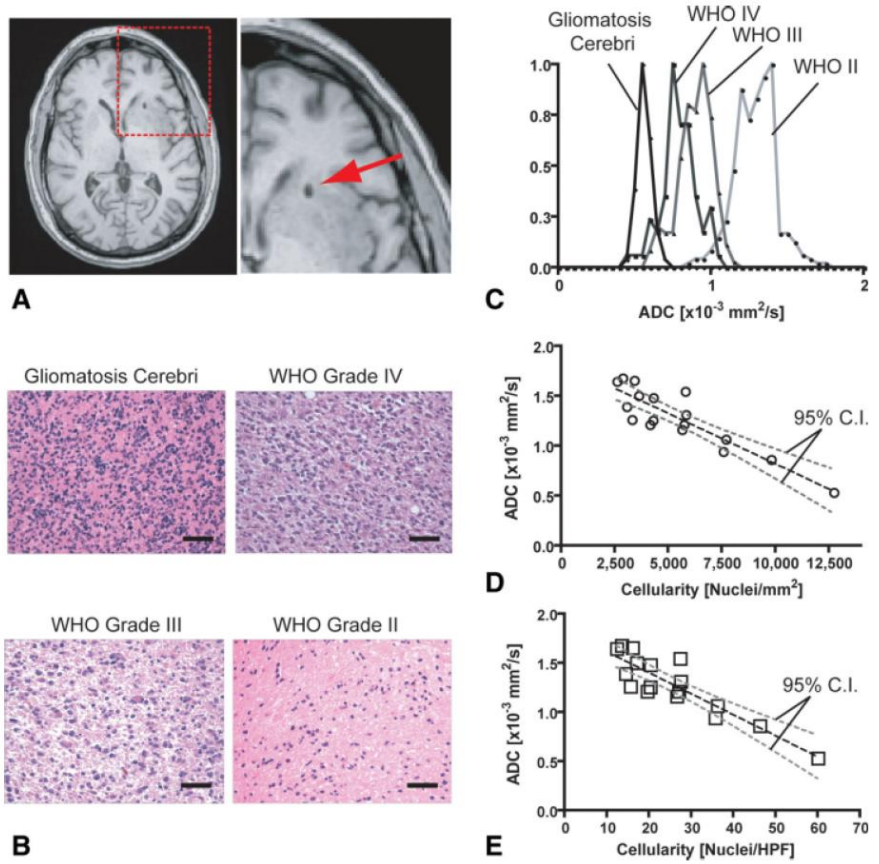

Figure 2. Correlation between spatially matched ADC measurements and cell density from stereotactic biopsy samples. **A:** Postoperative, high-resolution 3D T1-weighted anatomical MR images showing the biopsy location in a single patient. **B:** Representative histological images (hematoxylin & eosin, ×20 magnification) showing how cell density increases with an increase in tumor grade (scale bar = 50 μm). **C:** Spatially matched ADC measurements taken from the biopsy location in the same four patients as in B, showing a decrease in ADC with an increase in tumor grade and cell density. **D:** Scatter plot of average ADC within stereotactic biopsy locations and average cellularity for 17 patients (circles) shows a significant linear correlation (Pearson's correlation coefficient, $r^2 = 0.7933$; $P < 0.0001$) between mean ADC and mean cell density in nuclei/mm^2. **E:** Correlation between mean ADC and mean cell density in nuclei per HPF. Dashed black line = linear regression line; dashed gray lines = 95% confidence intervals for the regression.

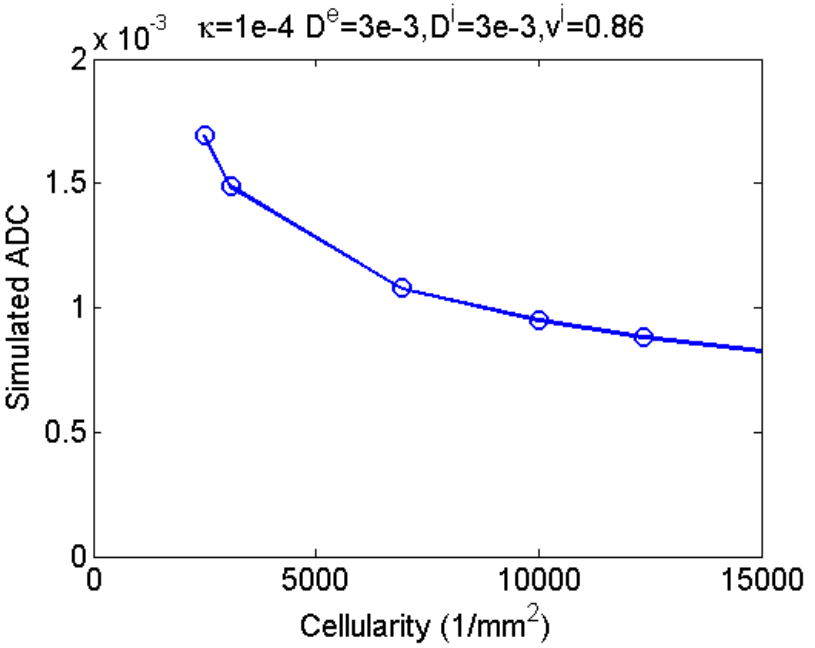

Simulation by FVforDMRI
ADC as a function of cell density

C++ version in development
Authors: Jing-Rebecca Li, Dang Van Nguyen

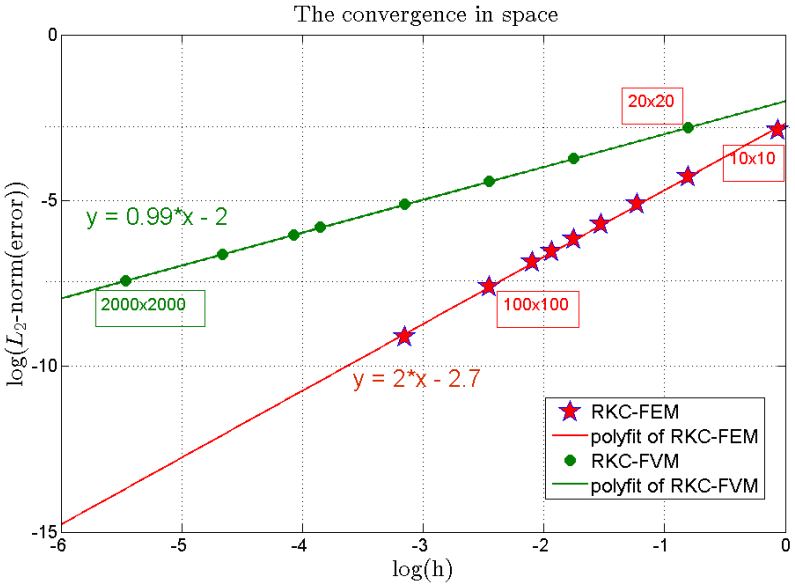

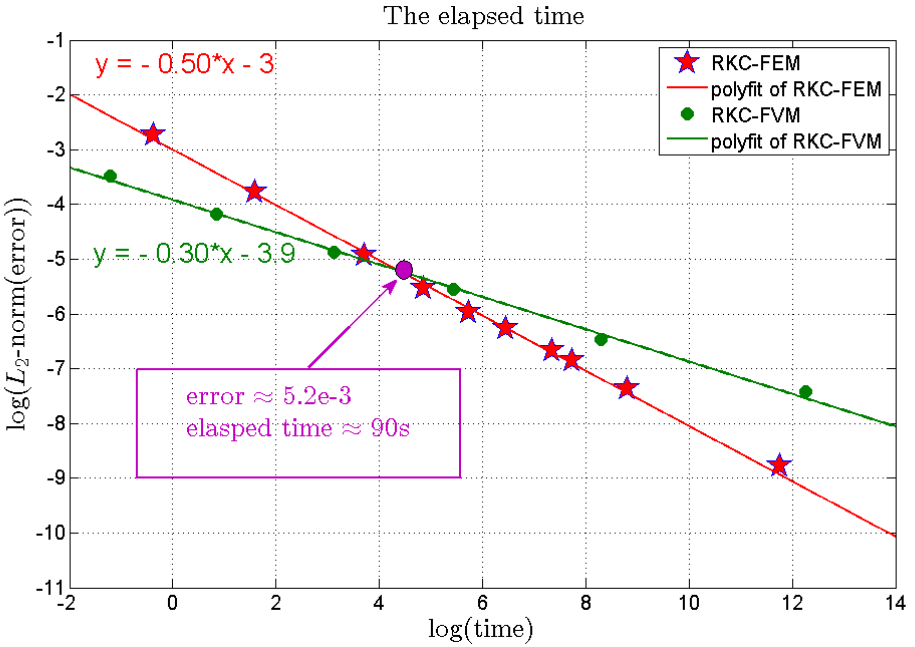

Benoit will speak about the Monte-Carlo code at the end

Planned work:

Antoine Lejay and Jing-Rebecca Li will define the interface condition to mimic permeability membranes to add to the Monte-Carlo code. Also add Green's function analytical solution for random walkers when they are far from any interfaces.

Step 2: Inverse problem.

- **Find reduced (ODE model), improved from existing model (Karger model)**

$$\frac{\partial \Psi^e(\vec{q},t)}{\partial t} = -c(t)D^e \parallel \vec{q} \parallel^2 \Psi^e(\vec{q},t) - \frac{1}{\tau^e}\Psi^e(\vec{q},t) + \frac{1}{\tau^i}\Psi^i(\vec{q},t)$$
$$\frac{\partial \Psi^i(\vec{q},t)}{\partial t} = -c(t)D^i \parallel \vec{q} \parallel^2 \Psi^i(\vec{q},t) - \frac{1}{\tau^i}\Psi^i(\vec{q},t) + \frac{1}{\tau^e}\Psi^e(\vec{q},t) \quad (1)$$

Step 2: Inverse problem

- **Solved inverse problem for average cell size, improved over Karger model.**
- **Numerically verified for simple geometry**

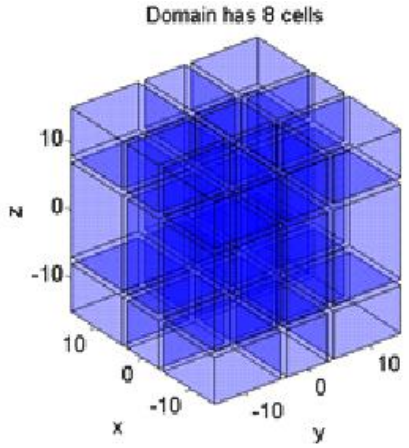

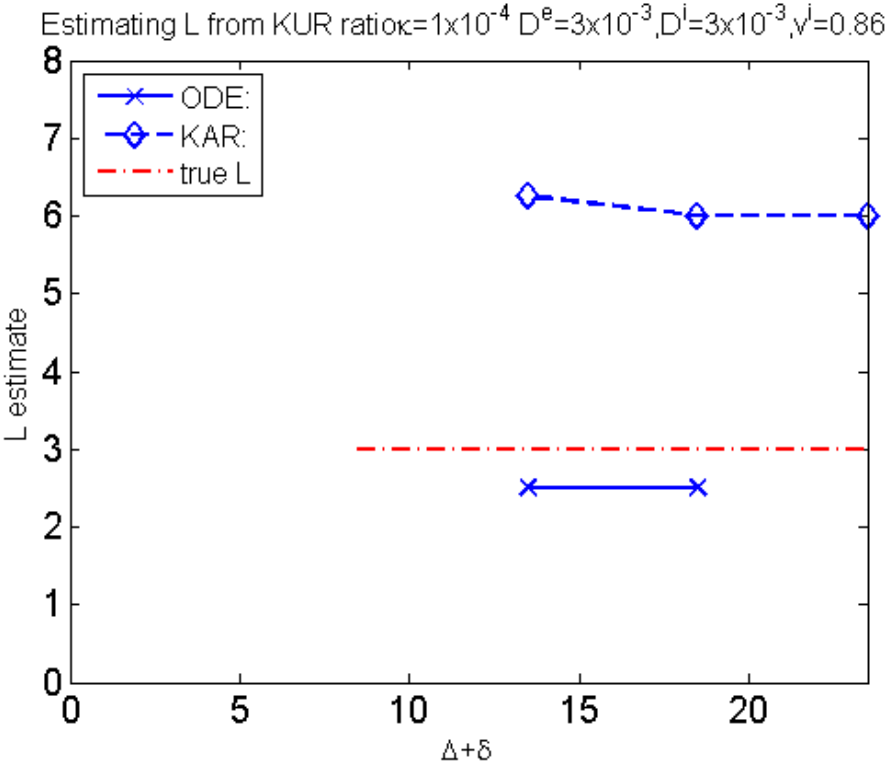

Step 3: Experimental verification (began Jan 2012)

- Imaging rat brains on the 17T Brucker small animal system at Neurospin.
- Preliminary experimental data have been obtained.
- Histology on the tissue samples is planned so as to provide the necessary geometrical parameters to input into the two codes.
- Reduced (ODE) model will be use to estimate average cell size.

Step 3: Experimental verification
Imaging rat brain

17T Brucker small animal system

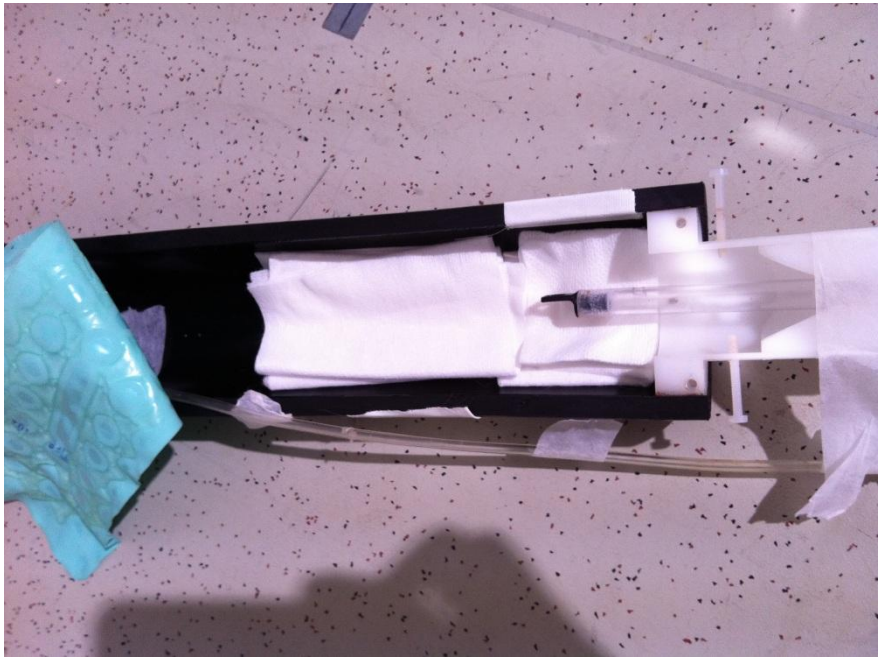

Imaging bed for rat

Step 3: Experimental verification

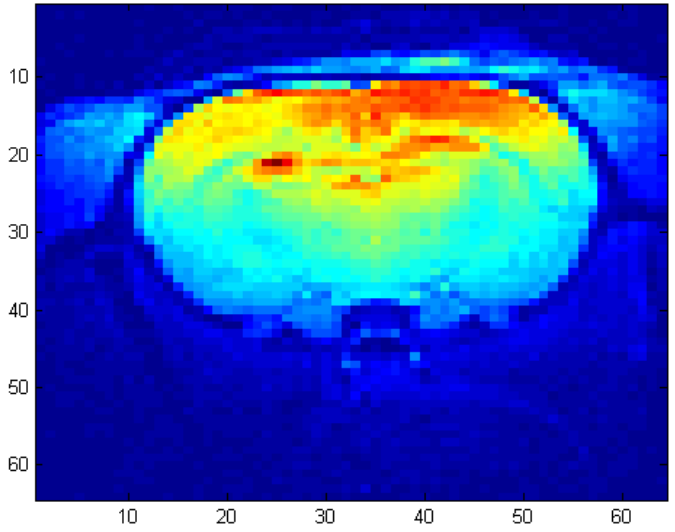

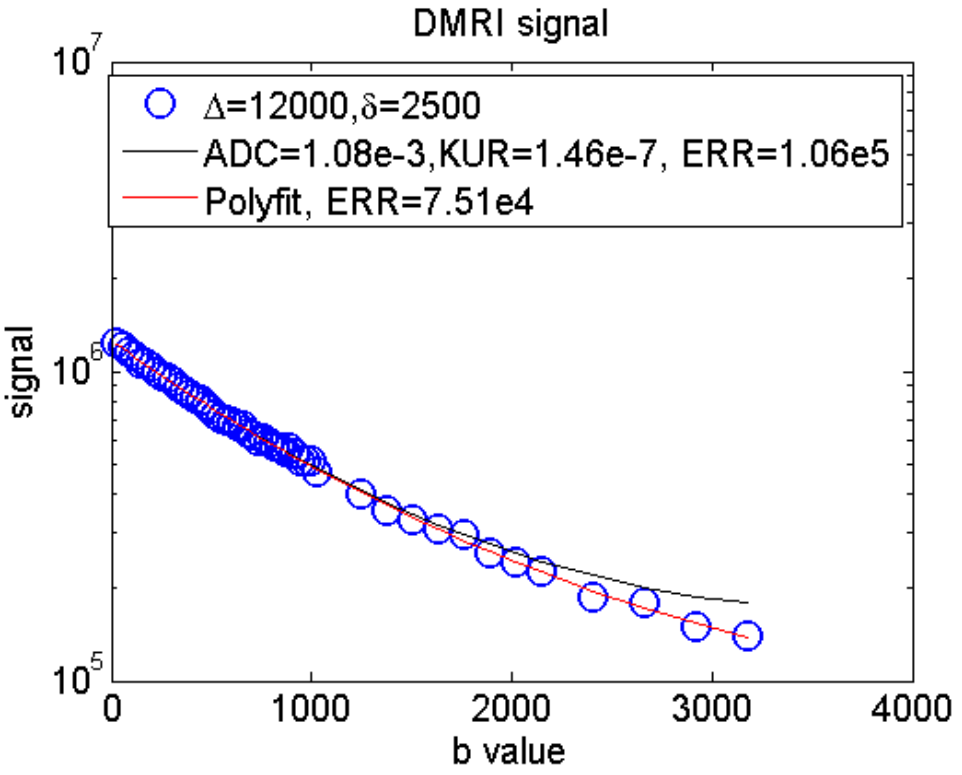

DMRI signal

Step 3: Experimental verification

- **Tumor model in rat**

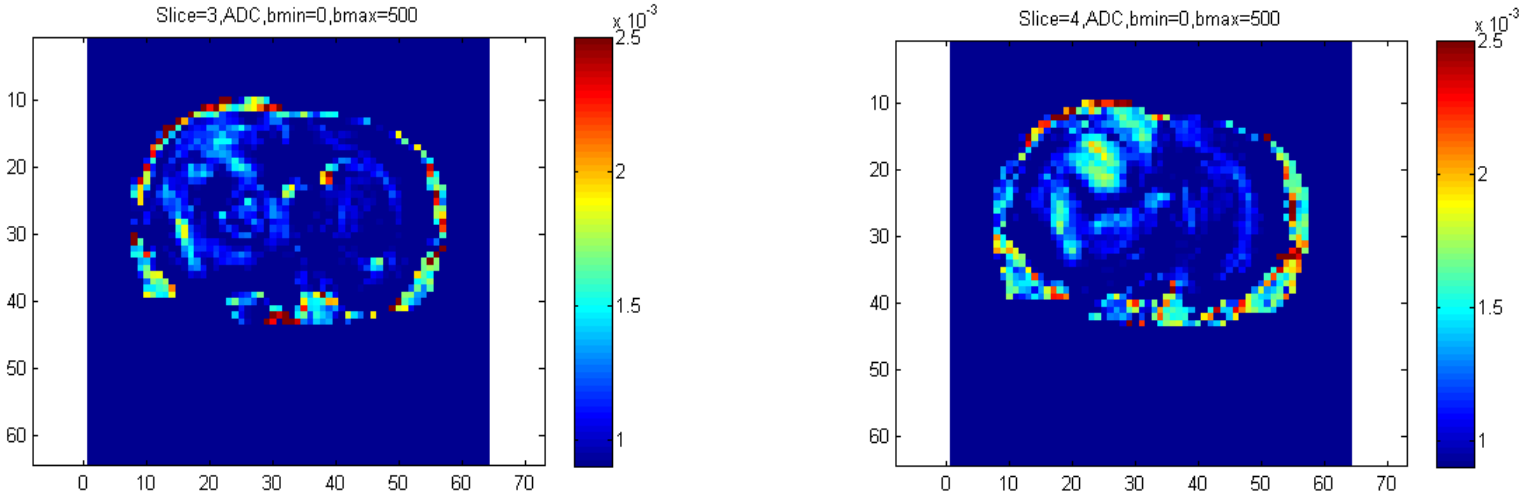

Imaging tumor in rat brain

Work program

1. Tache 1: The numerical method based on PDEs. It is written in Fortran90 and contains about 10000 lines. Completed.

2. Tache 1.1: Ph.D. student Dang Van Nguygen (funded by ANR) is implementing a C++. Ongoing.

3. Tache 2: New reduced ODE model can estimate cell size. Completed. Theory completed. Experimental verification ongoing.

4. Tache 3: Monte Carlo Brownian dynamics simulator capable of simulating diffusion of spins in arbitrarily complex geometries with a diffusion weighted signal integrator emulating various MR pulse sequences. Implemented in C++ on a high computing PC cluster for large-scale simulations. It contains 17000 lines of C++ code and 4000 lines of python code. Completed.

Work program

Tache 4: Imaging rat brains on the 17T Brucker small animal system at Neurospin. Preliminary experimental data have been obtained. Histology on the tissue samples is planned so as to provide the necessary geometrical parameters to input into the two codes. We plan to verify the simulation results of both the PDE method ('FVforDMRI') and the Monte-Carlo method ('Microscopist') against the experimental data obtained in rat brain on the 17T imaging system. Ongoing.

Tache 5: The Green's function formalism gives an interface condition that must be satisfied on the cellular membranes by any Monte-Carlo simulation so that the simulation results can be compared in a meaningful way with the PDE simulation results. This interface condition will be implemented in the Monte-Carlo code. We plan also to begin accelerate the Monte-Carlo code by incorporating known Green's function solutions in parts of the computational domain that are homogeneous. Planned.

Tache 6 : We have begun to evaluate different ways of acquiring sample brain geometries using electron microscopy in order to extract more realistic membrane geometries to be used as input to 'Microscopist'. Ongoing.

Joint (journal) publications

Li J.-R., Nguyen T.Q., Haddar H., Grebenkov D., Poupon C., Le Bihan D., Numerical and analytical models of the long time apparent diffusion tensor, preprint

Li J.-R., Nguyen H.T., Grebenkov, D., Poupon C., Le Bihan D., General ODE model of diffusion MRI signal attenuation, preprint

Li J.-R., Calhoun D., Poupon C., Le Bihan D., Efficient numerical method to solve the multiple compartment Bloch-Torrey equation, preprint

Yeh CH, Le Bihan D., Li J.-R., Mangin J.-F., Lin C.-P., Poupon C., Monte-Carlo simulation software dedicated to diffusion-weighted MR experiments in neural media. (Submitted to NeuroImage)

Yeh CH, Kezele I., Schmitt B., Li J.-R., Le Bihan D., Lin C.-P., Poupon C., Evaluation of fiber radius mapping using diffusion MRI under clinical system constraints. (Submitted to Magnetic Resonance Imaging)